Osteoarthritis and Cartilage 22 (2014) 323–333

Osteoarthritis and Cartilage

Subchondral chitosan/blood implant-guided bone plate resorption and woven bone repair is coupled to hyaline cartilage regeneration from microdrill holes in aged rabbit knees

J. Guzmán-Morales †, C.-H. Lafantaisie-Favreau ‡, G. Chen †, C.D. Hoemann †‡§*

† Department of Chemical Engineering, École Polytechnique, C.P. 6079 succ. Centre-Ville, Montréal, QC, Canada H3C 3A7
‡ Institute of Biomedical Engineering, École Polytechnique, C.P. 6079 succ. Centre-Ville, Montréal, QC, Canada H3C 3A7
§ Groupe de Recherche en Sciences et Technologies Biomédicales (GRSTB), École Polytechnique, C.P. 6079 succ. Centre-Ville, Montréal, QC, Canada H3C 3A7

ARTICLE INFO

Article history:
Received 8 May 2013
Accepted 10 December 2013

Keywords:
Bone marrow stimulation
Bone remodeling
Cartilage repair
Chitosan particles
Subchondral bone plate
Implant

SUMMARY

Objective: Little is known of how to routinely elicit hyaline cartilage repair tissue in middle-aged patients. We tested the hypothesis that in skeletally aged rabbit knees, microdrill holes can be stimulated to remodel the bone plate and induce a more integrated, voluminous and hyaline cartilage repair tissue when treated by subchondral chitosan/blood implants.

Design: New Zealand White rabbits (13 or 32 months old, $N = 7$) received two 1.5 mm diameter, 2 mm depth drill holes in each knee, either left to bleed as surgical controls or press-fit with a 10 kDa (distal hole: 10K) or 40 kDa (proximal hole: 40K) chitosan/blood implant with fluorescent chitosan tracer. Post-operative knee effusion was documented. Repair tissues at day 0 ($N = 1$) and day 70 post-surgery ($N = 6$) were analyzed by micro-computed tomography, and by histological scoring and histomorphometry (SafO, Col-2, and Col-1) at day 70.

Results: All chitosan implants were completely cleared after 70 days, without increasing transient post-operative knee effusion compared to controls. Proximal control holes had worse osteochondral repair than distal holes. Both implant formulations induced bone remodeling and improved lateral integration of the bone plate at the hole edge. The 40K implant inhibited further bone repair inside 50% of the proximal holes, while the 10K implant specifically induced a "wound bloom" reaction, characterized by decreased bone plate density in a limited zone beyond the initial hole edge, and increased woven bone (WB) plate repair inside the initial hole ($P = 0.016$), which was accompanied by a more voluminous and hyaline cartilage repair ($P < 0.05$ vs control defects).

Conclusion: In a challenging aged rabbit model, bone marrow-derived hyaline cartilage repair can be promoted by treating acute drill holes with a biodegradable subchondral implant that elicits bone plate resorption followed by anabolic WB repair within a 70-day repair period.

Introduction

Many patients needing cartilage repair therapy aged 40–65 years old, are considered too young for a joint replacement, and too old to respond well to standard therapies[1,2]. Treatments that work in skeletally immature rabbits (2–6 months old), which have a high spontaneous rate of regeneration compared to rabbits over 8 months old[3–6], may prove to be ineffective in middle-aged patient knees, which have low remodeling rates, declining mesenchymal stem cell populations, and low intrinsic capacity for chondrocytes to synthesize collagen type II[7]. Rabbits attain skeletal maturity with closed epiphyses at 7 months, but rabbits over 8 months old are needed to analyze osteochondral repair reactions in fully mature epiphyses[8].

In rabbit knees, drilled osteochondral defects of different diameter (0.9–3 mm) will spontaneously resurface with a soft fibrocartilage repair tissue, or occasionally form a depressed bone cyst[6,9–12]. Fibrocartilage contains mesenchymal stromal cells and chondrocytes embedded in an extracellular matrix of mixed collagen type I (Col-1) and collagen type II (Col-2) with low levels of glycosaminoglycan (GAG). A more hyaline cartilage can be elicited from subchondral bone defects, when a chitosan-glycerol phosphate/blood implant is flooded over the osteochondral defect surface, and solidified *in situ*[10,13].

* Address correspondence and reprint requests to: C.D. Hoemann, Department of Chemical Engineering, École Polytechnique, Montréal, QC, Canada H3C 3A7. Tel: 1-514-340-4848; Fax: 1-514-340-2980.
E-mail addresses: jessica.guzman-morales@polymtl.ca (J. Guzmán-Morales), charles-hubert.lafantaisie-favreau@polymtl.ca (C.-H. Lafantaisie-Favreau), gaoping.chen@polymtl.ca (G. Chen), caroline.hoemann@polymtl.ca (C.D. Hoemann).

1063-4584/$ – see front matter © 2013 Osteoarthritis Research Society International. Published by Elsevier Ltd. All rights reserved.
http://dx.doi.org/10.1016/j.joca.2013.12.011

However in rabbits >12 months old, the anabolic response to bone marrow stimulation is significantly attenuated, even with a bioactive chitosan-GP/blood implant[4].

To obtain a more potent cartilage repair response in skeletally aged knees, we previously developed a solid blood clot implant incorporated with chitosan particles, that is press-fit directly into a subchondral bone defect to attain a closer proximity between the implant and bone marrow-derived repair cells[14,15]. In a previous rabbit study carried to 3 weeks, it was shown that three pre-solidified implant formulations (10, 40, and 150 kDa chitosan) press-fit into adjacent trochlear drill holes induced local bone remodeling and delayed fibrocartilage deposition compared to control drill holes[14]. However, the 150 kDa chitosan/blood implant elicited significantly more apoptotic neutrophils that could potentially lead to a tissue void, and treated drill holes were encroaching upon each other[14]. Therefore, in this study, we used a two-hole drill model to test the hypothesis that pre-solidified blood implants containing rapidly degrading chitosan particles (80% degree of deacetylation (DDA), 10 kDa or 40 kDa) press-fit into microdrill holes, proceed to a phase of bone plate remodeling coupled to hyaline cartilage regeneration after 70 days, in rabbits >12 months old. This end-point was chosen based on the observation that microdrilled cartilage defects treated with an *in situ*-solidified chitosan/blood implant regenerate the subchondral bone to the osteochondral junction at 56 days post-operative[4,10]. In addition, given the anti-inflammatory properties of chitosan[16–18], post-operative knee effusion was documented.

Methods

Study design

All animal procedures were approved by institutional ethics review boards. Skeletally mature NZW rabbits (13 months old $N = 3$, 32 months old $N = 4$, 5♂, 2♀, 4.53 ± 0.67 kg, Charles River, St-Constant, QC, Canada) received two trochlear drill holes bilaterally. In one knee the holes were press-fit with a pre-solidified 40 kDa chitosan/blood (proximal) or 10 kDa chitosan/blood (distal) implant. The two contralateral drill holes were allowed to bleed as surgery-only controls. Mineralized and non-mineralized repair tissues were analyzed in initial defects ($N = 1$) and 70 days post-operative ($N = 6$).

Pre-solidified chitosan-NaCl/blood implant preparation

Chitosans (80–82% DDA, <500 EU/g, <0.2% protein, <5 ppm heavy metals, <0.2% ash) were obtained from BioSyntech (now Piramal Life Sciences, Laval, QC, Canada) and depolymerized by nitrous acid as previously described[19] to a target number-average molecular weight (M_n) of ~40 kDa, and ~10 kDa. Weight-average molecular weight (M_w), M_n and polydispersity index (PDI, M_w/M_n) were determined by size-exclusion chromatography (Table I). Chitosan powders were dissolved at 20 mg/mL in dilute HCl then autoclave-sterilized. Rhodamine-B isothiocyanate (RITC) labeled chitosans were generated at 1.0% mol RITC/mol chitosan from structurally matched 40 kDa and 10 kDa 80% DDA chitosans, dissolved in dilute HCl at 5 mg/mL and 90% protonation, 0.22 μm filter-sterilized, stored at −80°C and thawed once prior to use. Two isotonic 10 kDa or 40 kDa chitosan-NaCl formulations were prepared by combining chitosan-HCl and sterile NaCl solutions, then adding a 1:20 v:v ratio of 5 mg/mL RITC-chitosan of matching molecular mass, with a final osmolality of 292 mOsm (10 kDa chitosan-NaCl, termed "10K") and 318 mOsm (40 kDa chitosan-NaCl, termed "40K"). 250 μL aliquots of each formulation were distributed in flat-bottom 2.0 mL cryovials with three sterile 0.39 g surgical steel mixing beads (Salem Specialty Ball, Canton, CT, USA). At surgery, 0.75 mL–1.5 mL of fresh aseptic peripheral arterial autologous whole blood was added, the cryovials shaken manually for 10 s, the liquid mixtures drawn into sterile depyrognized borosilicate glass tubes (2 mm inner diameter), and coagulated for 20–60 min at 37°C. Implants were extruded onto a sterile petri dish, trimmed with a scalpel to insert in the defects, and left-over pieces fixed in formalin to document chitosan particle formation and dispersion by epi-fluorescence microscopy.

Table I
Chitosan powders used to generate pre-solidified implants

Chitosan powder	DDA (%)	M_w (kDa)	M_n (kDa)	PDI*
40K†	80.2	48.8	37.7	1.3
RITC-40K‡	81.3	61.5	46.7	1.3
10K†	81.9	23.8	12.7	1.9
RITC-10K‡	80.0	22.4	12.4	1.8

* PDI (M_w/M_n).
† Chitosan powder used to make the 20 mg/mL autoclave-sterilized solution.
‡ RITC-chitosan powder used to make the 5 mg/mL filter-sterilized solution.

Rabbit osteochondral repair model

Rabbits were anaesthetized with ketamine-xylazine-buprenorphine, had their knees shaved and disinfected, and were maintained with 3% isoflurane/8% oxygen. Small bilateral arthrotomies were made one knee at a time and the trochlea exposed by medial patellar displacement. At two equally spaced sites in each femoral trochlea, the cartilage was debrided, then microdrilled to 2 mm deep using a 1.4 mm-diameter round drill burr (Fine Sciences Tools, Foster City, CA, USA) under constant irrigation with Ringer's Lactated Saline to rinse away bone powder. Holes were left to bleed [Fig. 1(A)], or press-fit with a ~2 mm implant piece, 40K and 10K, by gently pushing with a sterile p200 pipetman tip from 10 to 25 times to fully embed the implant [Fig. 1(B)]. Knees were closed in three layers, and rabbits allowed immediate unrestrained cage activity. One female rabbit (6.4 kg, 32 months old) had an unscheduled death immediately after surgery due to complications from anesthesia, and the femur ends were collected and analyzed as initial defects (D0). Buprenorphine was administered post-operatively twice a day for at least 3 days as needed. Safety was monitored by body weight and observations of knee pain and effusion. Knee effusion was monitored by two observers during 70 days and scored on a scale of 0–4: 0 = no effusion, 1 = slight knee swelling, 2 = clear effusion or swelling, 3 = a lump, and 4 = a very large lump (≥1.5 cm diameter) over or near the surgical sutures. Daily scores were averaged in each group of rabbits ($N = 6$) and graphed vs the day post-surgery up to day 40. The area under the curve was then calculated using a trapezoidal rule. The cumulative knee effusion score was plotted using Prism 6 (GraphPad, La Jolla, CA, USA). Rabbits were euthanized at day 70 under anesthesia by IV injection of sodium pentobarbital and the femoral ends fixed in 4% paraformaldehyde/100 mM cacodylate, pH 7.4. Femur ends and cryosections were analyzed by inverted epifluorescent microscopy (Northern Eclipse, Empix, Mississauga, ON, Canada), for fluorescent chitosan. Defects were scored for macroscopic appearance using digital images acquired with a dissection microscope [Fig. 1(C and D)], based on the following tissue color grading: 1 = depression (tissue void), 2 = red/grey, 3 = beige, 4 = red–white, and 5 = white, homogeneous tissue.

Micro-computed tomography (micro-CT)

Femur ends trimmed of their condyles were micro-CT scanned (SkyScan1172, Skyscan, Kontich, Belgium) at an image size of 2000 × 1048 pixels, pixel size resolution 9.8 μm, two-frame

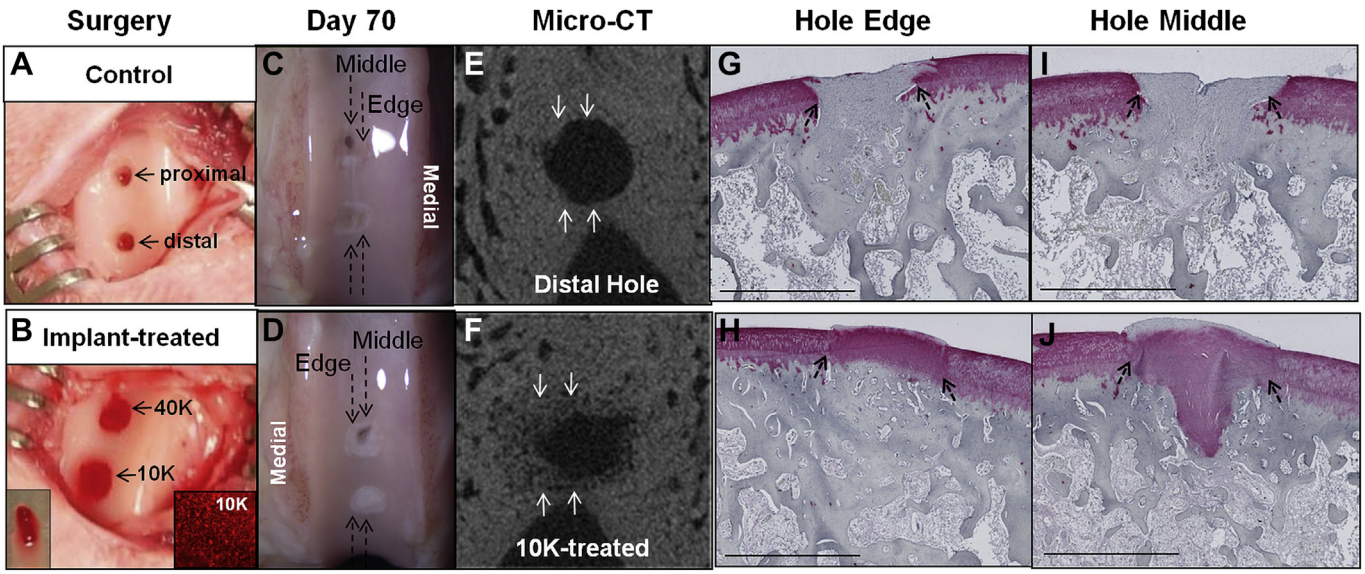

Fig. 1. Mature rabbit cartilage repair model of subchondral chitosan/blood implant-guided osteochondral repair and experimental approach. Representative drill-only control defects (A, C, E, G, I) and implant-treated drill-holes (B, D, F, H, J) at surgery (A, B), and day 70 post-operative showing an axial view by micro-CT of residual hole area (E, F), and sagittal cryosections at the hole edge and middle stained for Col-2 (G–J, dotted arrows point to the limits of the initial drill holes). Insets in panel B: representative images of a trimmed chitosan-NaCl/blood implant prior to press-fitting in the drill hole, and fluorescent images of left-over implant segments showing dispersed RITC-chitosan microparticles (5× magnification). Abbreviations: 40K and 10K = 40 kDa and 10 kDa chitosan/blood pre-solidified implant. Arrows (C–F) indicate the approximate area at the hole edge and middle where sections were collected according to the histology staining plan. Scale bar (G–J): 2 mm.

averaging, 180° rotation at 80 kV with an aluminum-copper filter. Data sets were reconstructed in a 3D model (NRecon Skyscan software, smoothing: 2, ring artifact correction: 6, beam hardening correction: 30%, object bigger than field of view: off) and blinded by a third party. To determine hole depth, each drill hole was re-positioned in an axial view to toggle depthwise through the hole [DataViewer Skyscan software, Fig. 1(E and F)], and the number of 2D slices was counted from the top to the bottom of each hole, then multiplied by the pixel size (9.8 μm/slice)[14]. Residual bone hole cross-sectional area at the hole surface and at three different depths (−0.5, −1.0 and −1.5 mm) was quantified by using a polygonal tool (CTAn Skyscan software) to draw a 2D region of interest (ROI) in the axial plane that circumscribed the non-mineralized hole edge, using an inverted 70–0 threshold to capture non-mineralized tissue area[14]. A novel measurement was developed to quantify the previous events of bone plate resorption and repair – also termed "wound bloom"[4,14], by quantifying a reduction in the mineralized tissue density in the area immediately flanking the top of the initial microdrill hole at day 70 post-operative vs day 0. The 2D bone area fraction (bone area/tissue area, %) was measured in two concentric circular ROIs centered over each residual hole, with a diameter of 1.43 mm ("inside drill hole"), and 2.00 mm (maximal diameter of observed bone remodeling "outside drill hole", 75–255 threshold). The bone area fraction surrounding the initial drill hole was then obtained by subtracting bone area fraction (%) "inside drill hole" from the bone area fraction (%) "outside drill hole". To quantify the mineralized repair tissue integration with flanking native subchondral bone plate, a circular ROI of 1.44 mm diameter was placed at the top of the axial view of each drill hole, and with a 75–255 threshold, the attachment percentage of bone outside to bone inside the initial hole was calculated using the following formula: Attachment % = Intersection perimeter (mm)/Tissue perimeter (mm) × 100.

Histoprocessing and histomorphometry

After micro-CT, femoral ends were decalcified at 4°C in 10% ethylene diamine tetraacetic acid (EDTA)/0.1% paraformaldehyde/PBS pH 7.2. Using calibrated macroscopic images and a Leica digital cryostat to precisely trim into the cryoblock, serial 10 μm sagittal cryosections were collected with CryoJane tape (Instrumedics, St Louis, MO, USA) at the medial edge (hole edge) and through the middle (hole middle) of the two drill holes [Fig. 1(G–J)]. Sections were stained with Safranin O-fast green-iron hematoxylin (SafO), or immunostained with anti-human Col-1 antibody I-8H5 (MP Biomedicals, Solon, OH, USA, 10 μg/mL) and anti-human Col-2 hybridoma supernatant II6B3 (DSHB, Iowa City, IA, USA, ~7.5 μg/mL), biotinylated goat anti-mouse secondary antibody (B-7151; Sigma–Aldrich, Oakville, ON, Canada, 11 μg/mL), and ABC red substrate detection (Vector, Cedarlane Mississauga, ON, Canada). Isotype-matched control IgGs and primary antibody omission showed no background staining. Quantitative histomorphometry was carried out by one trained and blinded observer on calibrated 2.5× magnification images exported from 40× digital slide scans. The total chondral repair tissue area (mm^2), including bone overgrowth, was quantified on cropped regions of interest encompassing all repair tissue above the osteochondral junction as determined from the projected tidemark in flanking cartilage. Percentage SafO, Col-1 or Col-2-positive stained tissue (excluding bone overgrowth), was obtained by thresholding using Image J (National Institutes of Health, Bethesda, MD, USA), followed by an in-house Matlab routine (V. 7.5.0.342 Mathworks, Natick, MA, USA)[20]. Modified O'Driscoll scoring[21] was performed by two blinded readers using SafO stained cryosections. Subchondral Col-1 fiber organization was analyzed by polarized light microscopy (PLM).

Statistical methods

Results are presented as mean ± 95% confidence interval (C.I.). Mann–Whitney *U* test was used to test the effect of implant vs control on macroscopic scoring, para-patellar effusion and modified O'Driscoll. Using drill hole as the statistical unit, the General Linear Model (GLM, Statistica version 9.0, StatSoft, Tulsa, OK, USA) with Fisher LSD post-hoc analysis was used to analyze differences between conditions ($N = 6$, 40K, 10K, proximal, distal; $N = 4$, initial defects). $P < 0.05$ was considered significant.

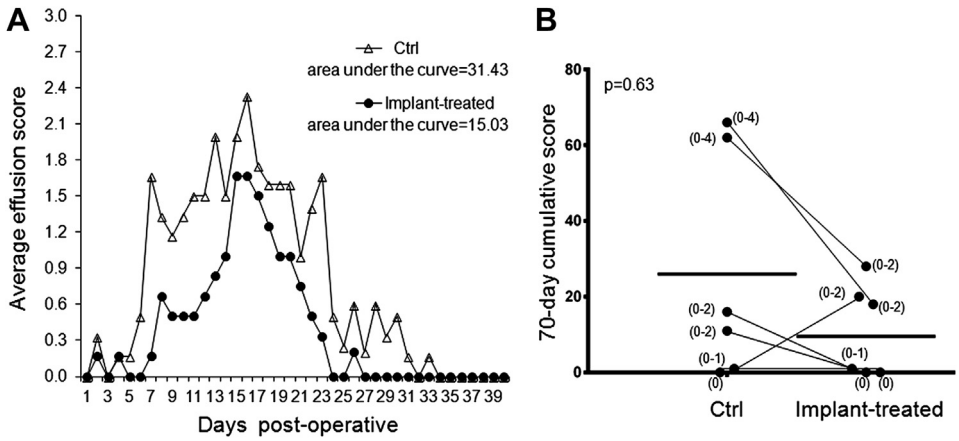

Fig. 2. Bilateral knee effusion scores were monitored post-surgery in rabbits, and data shown as average daily effusion scores over 40 days post-operative ($N = 6$ per timepoint, A) and as cumulative inflammation scores over 70 days of repair per rabbit knee (B). In panel B, paired results per rabbit are represented (black circle), with the min–max per knee given in parentheses, and the mean per group showed by a horizontal line ($N = 6$). Effusion scores were lower for five out of six implant-treated knees vs control knees (Ctrl).

Results

Macroscopic appearance of cartilage in relation to histological score and knee effusion

In control knees, effusion appeared around day 7, was sustained until day 21, and resolved by day 35 [Fig. 2(A)]. In implant-treated knees, effusion had a more gradual onset, peaked at around day 14, and resolved by day 28 [Fig. 2(A)]. Implant-treated knees showed consistently lower post-operative knee effusion compared to drill-only contralateral knees, but the effect was not significant [Fig. 2(B)].

After a 70-day repair period, all drill holes were filled with connective tissue, except for one control and three treated defects with a visible tissue void in the middle of the defect [Fig. 3]. Tissue void in four microdrill holes was observed in knees with an effusion score over 17 [white text, Fig. 3(A–L)]. White connective tissues filled most of the distal holes, with better overall macroscopic scores, and higher total modified O'Driscoll histological scores than proximal defects which had a heterogeneous color [black text, Fig. 3(A–L)]. One red–grey tissue had a cyst below the cartilage repair [arrowhead, Fig. 3(K)]. At 70 days post-operative, all fluorescent chitosan was cleared from the implant-treated holes (data not shown).

Soft tissue and mineralized bone repair

By micro-CT measures, initial microdrill holes had a reproducible 2 mm depth, that 70 days post-surgery, was diminished to ~1 mm deep for control defects, and ~1.7 mm deep for implant-treated defects [Fig. 4(A–C and P)]. At the hole surface, the initial defect and control defects had the same cross-sectional area [Fig. 4(Q)], revealing a lack of bone plate remodeling. Residual holes in control defects were often filled with fibrous soft tissue or a void [Fig 4(D–F)], or a sprouting osteochondral unit [Fig. 4(G–I)]. Many implant-treated drill holes had a pear-shape [Fig. 4(C)], indicating a side-wall remodeling and repair took place in the trabecular bone area. Bone plate remodeling, only observed in implant-treated holes, was sometimes associated with a bone cyst void [2, 40K- and 1, 10K-treated hole, Fig. 4(J–L)], or with chondroinduction [4 out of 6 10K-treated holes, Fig. 4(M–O)]. 10K-treated drill holes had a significantly smaller residual bone hole area at the surface, compared to matching distal drill-only defects [$P = 0.033$, Fig. 4(Q)].

Previous events of bone plate resorption, repair, and integration were measured on bone flanking the initial hole surface [dashed circles, Fig. 5(A–C)]. The bone area fraction outside the drill hole declined from ~36% at surgery, to ~21% for control drill holes, and ~8% for 40K and 10K implant-treated holes [$P < 0.001$ vs control holes, $N = 6$, Fig. 5(D)] at day 70. These data demonstrate that chitosan/blood implants elicited stronger prior remodeling of bone plate outside the initial hole. Only 10K-treated bone holes [Fig. 5(C)] showed a higher bone area fraction inside the hole [$P = 0.016$ vs initial hole, Fig. 5(D)]. Implant-treated holes showed significantly higher lateral bone integration at the bone plate, compared to control drill holes [~10% and ~16% for 40K- and 10K-treated holes, respectively vs 2.5%, Fig. 5(E)]. All these results taken together indicate that a "wound bloom-like" process had specifically occurred in the bone plate of microdrill holes treated with pre-solidified 10K implants, that is, an incremental increase in wound size, followed by bone repair with improved integration with surrounding trabecular bone.

At the hole edge of treated drill defects, bone remodeling leading to a more porous bone structure was paralleled by higher cartilage repair tissue Col-2%, and higher total modified O'Driscoll scores [$P < 0.05$, Fig. 5(D and F–H)], partly due to a consistently higher hyaline nature and structural integrity of the repaired cartilage. In the middle of the holes, no significant differences were detected due to implant treatment [Fig. 5]. 10K implants did not induce specific degenerative changes in adjacent native cartilage (Table II). In implant-treated defects, the total modified O'Driscoll scores were higher in sections from the hole edge than in the middle (Table II), which is consistent with an "outside-in repair". Conversely, the control defects had higher repair score in the hole middle than in the edges [Fig. 5(G), Table II], partly due to the "sprouting" of control tissue from the hole with poor lateral integration, and reduced SafO staining of the matrix. Proximal holes had significantly lower total histological scores than distal holes at the edges [Fig. 5(G), Table II].

When comparing distal repair tissues in the same animal, the 10K implant reproducibly elicited better osteochondral integration, compared to the contralateral control [thin black arrows, Fig. 6(A–E); Supplemental Fig. 1]. 10K-treated repair tissues also delayed chondrocyte hypertrophy that was evident in control repair tissues [Fig. 6(A–F)]. Overall, 10K treatment stimulated an increase in repair tissue fill vs 40K-treated holes, and vs distal control holes [Fig. 6(G)]. Proximal drill holes showed the least repair tissue fill [Prox, 40K, Fig. 6(G)]. 10K-treatment elicited a hyaline-like cartilage

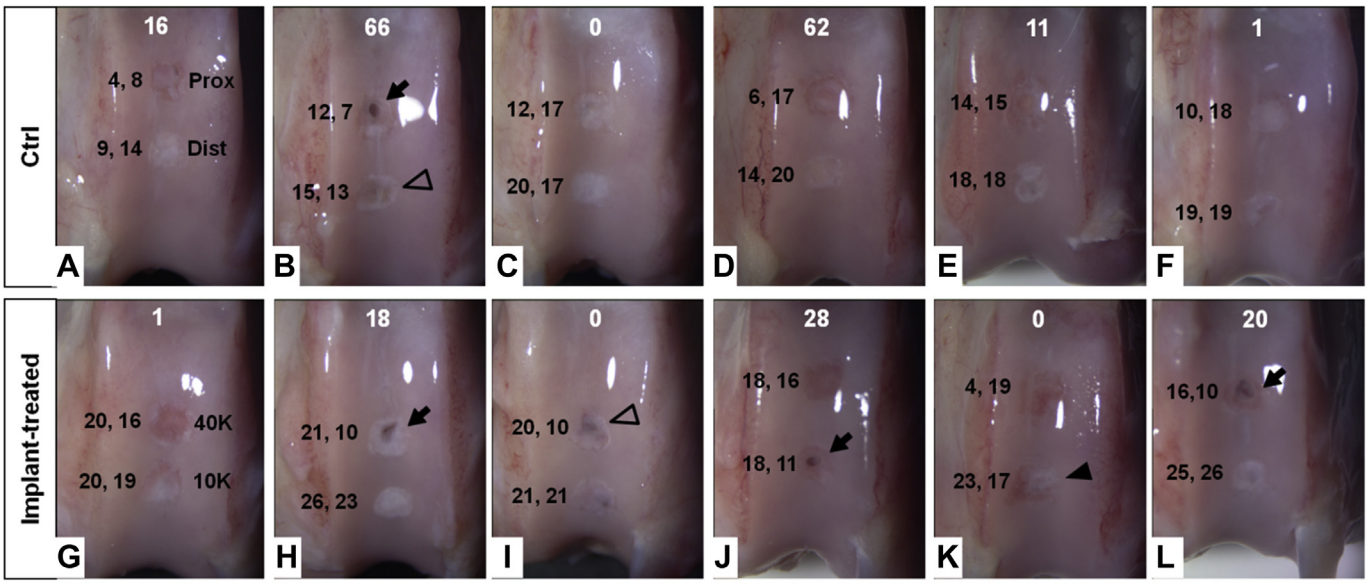

M

Macroscopic score

	Prox	40K	Dist	10K
White homogeneous (5)	2	0	5	4
White-red (4)	0	0	0	1
Beige (3)	3	0	1	0
Red-grey (2)	0	4	0	0
Tissue void (1)	1	2	0	1
Average (± 95% C.I.)	3.3 (±1.2)	1.7 (±0.4)*	4.7 (±0.7)	4.2 (±1.3) #

* *vs* Prox, p=0.038, # *vs* 40K, p=0.037

Panels A-L

White values: total knee inflammation score

Black values: Total modified O'Driscoll (hole edge, hole middle)

Tissue void

Soft tissue depression

Subchondral bone cyst

Fig. 3. Macroscopic appearance (Panels A–L) of drill-only control defects (Ctrl; upper panels) with corresponding contralateral implant-treated defects (lower panels), and macroscopic scores (M, average ± 95% confidence intervals, $N = 6$). Abbreviations: Prox: proximal defect, drill-only; Dist: distal defect, drill only; 40K: 40 kDa chitosan/blood implant-treated proximal defect; 10K: 10 kDa chitosan/blood implant-treated distal defect.

repair tissue in five out of six defects, with an extracellular matrix containing ≥60% of SafO positive tissue, and more GAG at the hole edge vs distal control holes and vs 40K-treated holes [$P < 0.005$, white bars, Fig. 6(H)]. Col-1 was present in around 20% of the chondral repair tissue regardless of the treatment [Fig. 6(I)].

At the repair cartilage–bone interface of many treated defects, blood vessels surrounded by woven bone (WB) were observed close to the soft repair tissue whereas lamellar bone (LB) containing organized Col-1-positive bone fibers was observed deeper into the holes [Fig. 7(A)]. WB was recognized histologically as having more abundant and larger osteocytes inside a disorganized Col-1 matrix [Fig. 7(B)]. To summarize, implant-induced bone remodeling at the hole edge was paralleled by increased Col-2-positive repair tissue over areas of remodeled bone, while differences in repair quality in the middle of the hole due to implant treatment were mainly qualitative, including less hypertrophic cartilage than control defects. The 10K implant elicited superior cartilage repair at the defect edge where bone resorption and repair has taken place.

Discussion

This study is the first to report that subchondral pre-solidified ultra-low M_w chitosan/blood implants can significantly enhance the volume of hyaline cartilage repair elicited from osteochondral microdrilled defects, in rabbits aged above 1 year old. This is in contrast with chitosan/blood implants that solidify *in situ* above the osteochondral defects and elicit a limited healing response in old rabbits[4]. These data represent an important advance in the conception and design of new cartilage repair therapies to treat middle-aged patients. Microdrill holes used as surgical controls generated a commonly-observed spontaneous repair of a semi-isolated unit growing from the bottom-up with fibrous or fibrocartilage character, as reported by many studies using skeletally mature and immature rabbits[3,4,6,13]. Therefore, maturation of the fibrocartilage repair tissue previously observed at 21 days post-operative in control defects in a similar model[14] was not further improved by a longer 70-day repair period in this study.

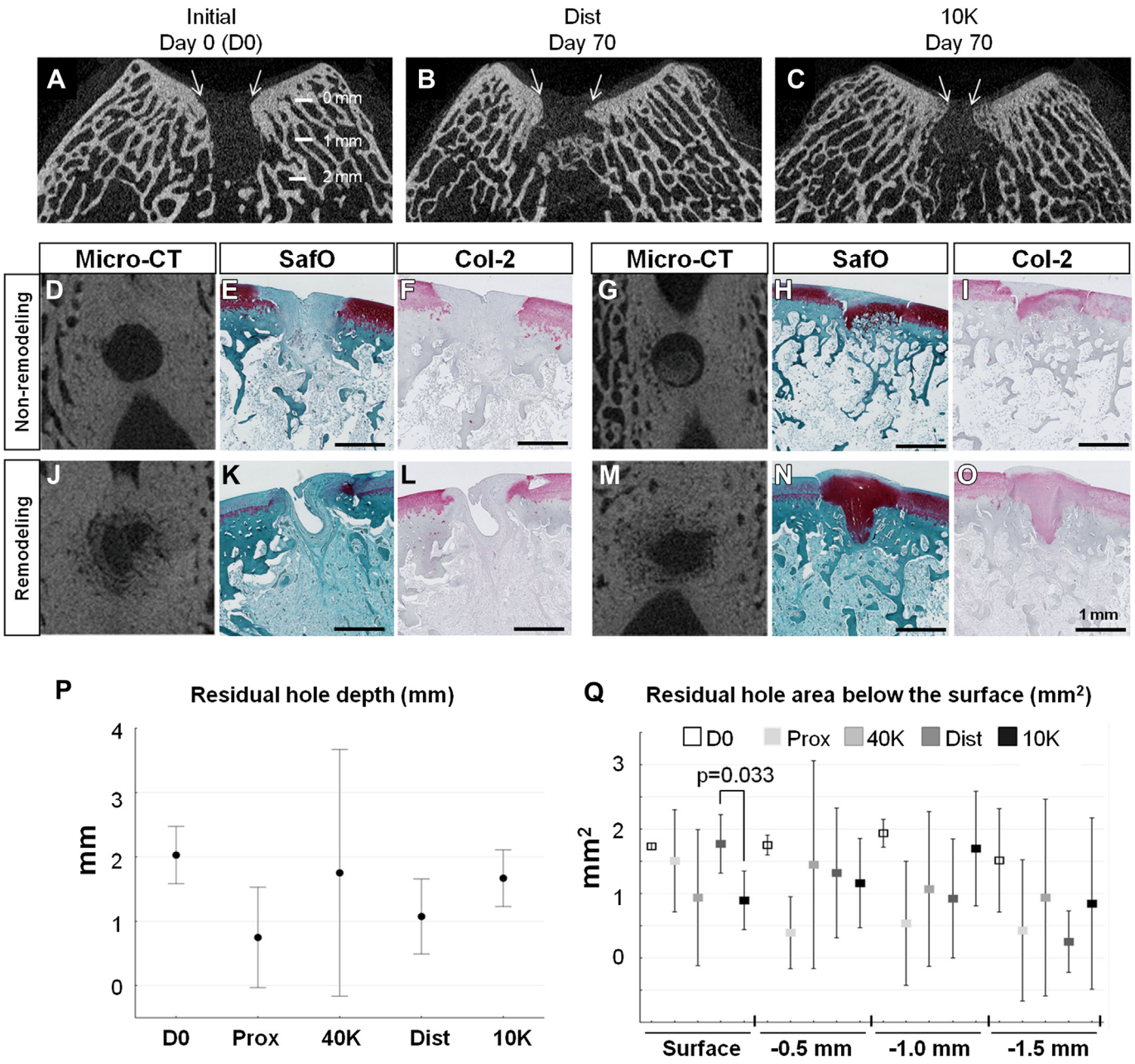

Fig. 4. Influence of chitosan implant on drill hole bone remodeling and residual bone hole dimensions at 70 days post-operative. Representative transverse views by micro-CT of residual drill hole at day 0 (A), and day 70 post-operative (B, drill-only, C, 10K-treated). Different soft tissues were associated with residual bone holes (micro-CT axial views and histology at the hole middle), including fibrous tissue (D–F, control), fibrocartilage sprouting (G–I, control), depressed tissue (J–L, 40K-treated) and subchondral cartilage (M-O, 10K-treated). Micro-CT measures of average residual bone hole depth (P) suggest WB repair at the base of most holes. Bone hole diameter at specific depths (Q) revealed a significantly smaller hole at the surface of 10K-treated drill holes. $N = 4$ D0, $N = 6$ Day 70 Prox, 40K, Dist, 10K.

Biodegradable chitosan-NaCl/blood implants press-fit into drill defects remain in the defect for a few weeks and induce an incremental increase of the bone lesion size filled with granulation tissues containing neutrophils and stromal cells; at 21 days post-operative, WB ingrowth into angiogenic granulation tissue at the hole edges was evident[14]. Data in this study show that implant-induced osteoclast activity is followed by mineralized tissue repair during the closure of the bone wound [Fig. 5]. This "wound bloom" effect[4,20] promotes anatomical incorporation of regenerated tissue to the native osteochondral unit [Fig. 8]. Specifically in 10K implant-treated distal defects, further bone plate repair was coupled to bone-plate guided chondroinduction. Better integration of the repair tissues to the native osteochondral unit could drive an improved repair response, by juxtaposing bone mesenchymal stromal cells (BMSCs) with native chondrocytes. Co-cultures of BMSCs with chondrocytes were previously shown to increase chondrogenesis and inhibit hypertrophy, illustrating the mutual beneficial effect of close proximity of these cell types[22]. In addition, better lateral integration of the soft chondral repair tissue with native cartilage ("Bonding", Table II) could partly explain the more hyaline repair in many implant-treated holes, as primary chondrocytes release paracrine factors that can induce de-differentiated passaged chondrocytes to express collagen type II[23].

Bone resorption preceding bone formation has also been reported after the administration of bone morphogenetic protein 2

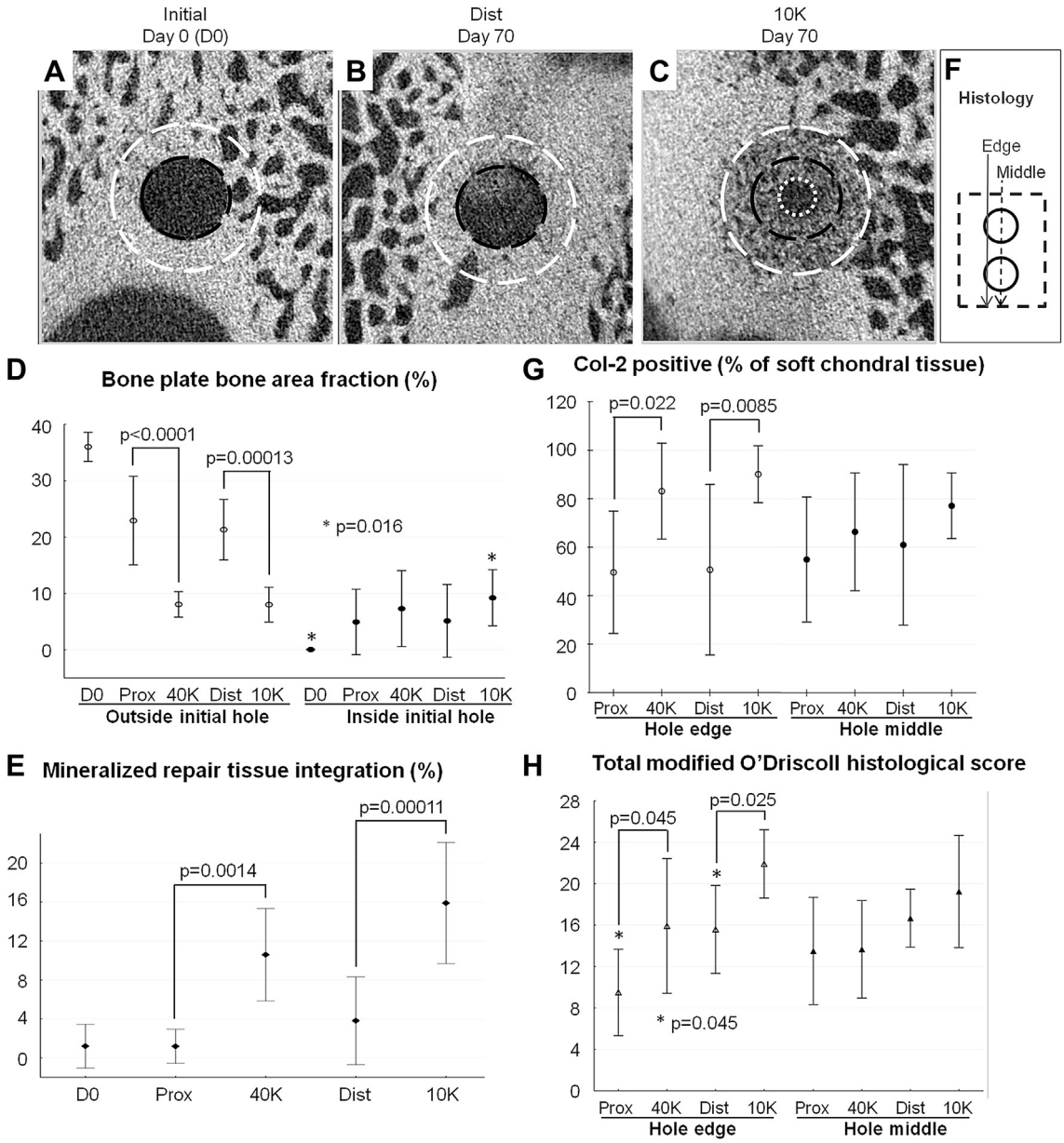

Fig. 5. Novel micro-CT measures of previous bone resorption and repair show that bone plate remodeling, repair, and mineralized tissue integration is coupled with Col-2 accumulation and improved histological repair tissue quality. (A–C) Axial micro-CT images at the bone plate level, (D) bone plate area fraction, and (E) bone repair tissue lateral integration in relation to cartilage repair histomorphometry through the edge and the middle of the holes (F), for (G) % Col-2-positive soft tissue repair above the osteochondral junction and (H) total modified O'Driscoll score. $N = 4$ D0, $N = 6$ Day 70 Prox, 40K, Dist, 10K. Panels A–C: black dotted circle: initial drill hole perimeter; white large dotted circle: limits of the new bone formed after remodeling; white small dotted circle: remaining unrepaired hole perimeter in implant-treated defect.

(BMP-2) in an absorbable collagen sponge[24], and this sequence of events (bone resorption followed by bone formation) is characteristic of the remodeling occurring naturally in bone biology[25]. By contrast, delivery of TGF-β and BMP-4 in an alginate implant was reported to induce cartilage repair without inducing bone remodeling in an 8 month-old rabbit drill model[26]. One advantage of the chitosan implant approach described here is that it is a cell-free biomaterial device and does not require added biologics -whose dosages are challenging to identify for different-size defects. The subchondral chitosan implant shows great potential as a therapeutic cartilage repair device, although more studies are needed as the 40K implants also induced bone remodeling but most frequently failed to regenerate the bone plate and a hyaline cartilage tissue after 70 days. The tissue voids and fibrous repair tissue present in most 40K-treated defects are not predicted to transform to hyaline cartilage with longer repair periods. Slower clearance rates of the polydisperse 40K chitosan[14] may have prolonged the osteoclast recruitment phase resulting in repair failure. These results altogether suggest that a strong bone plate resorptive phase can only promote hyaline repair when followed by a strong WB repair phase maturing into LB within a specific time frame, in aged animals. Cartilage repair tissue integrated with a mineralized bone plate is also expected to be a more durable repair tissue. A microdrilling study in the 90's reported that skeletally mature rabbit cartilage repair tissue that retained its integrity beyond a 36-week repair period of full-thickness defects were those in which the subchondral bone had been reconstituted to its normal gross architecture[6].

Table II
Modified O'Driscoll scoring

	Hole edge				Hole middle			
	Prox	40K	Dist	10K	Prox	40K	Dist	10K
1. Nature of predominant tissue								
Cellular morphology								
(4) Hyaline Articular Cartilage	0	0	0	2	0	1	1	1
(3) Fibrocartilage	1	5	3	4	3	2	3	4
(2) Incompletely differentiated mesenchyme	0	0	0	0	0	0	2	0
(1) Fibrous tissue	4	0	3	0	3	3	0	0
(0) Bone	1	1	0	0	0	0	0	1
Safranin O staining of the matrix								
(3) Normal or nearly normal	0	0	0	2	0	1	1	2
(2) Moderate	0	1	2	2	0	0	2	1
(1) Slight	0	2	1	2	2	2	1	3
(0) None	6	3	3	0	4	3	2	0
2. Structural characteristics								
Surface regularity								
(3) Intact	0	4	3	2	2	1	2	1
(2) Superficial horizontal lamination	2	0	1	1	2	1	2	3
(1) Fissures 25–100% of thickness	2	1	2	3	1	1	1	1
(0) Severe disruption in including fibrillation	2	1	0	0	1	3	1	1
Structural integrity								
(2) Normal	0	5	1	6	0	2	0	4
(1) Slight disruption, including cysts	1	0	1	0	4	1	4	2
(0) Severe disintegration	5	1	4	0	2	3	2	0
Thickness								
(2) 00% of normal	1	2	4	4	2	0	4	4
(1) 50–100% of normal	2	2	2	2	2	2	2	2
(0) 0–50% of normal cartilage	3	2	0	0	2	4	0	0
Bonding to adjacent cartilage								
(2) Bonded at both ends	1	2	2	5	2	6	2	5
(1) Bonded at one end or partially at both ends	2	2	2	1	1	0	4	1
(0) Unbonded	3	2	2	0	3	0	0	0
3. Freedom from structural changes of degeneration								
Hypocellularity								
(3) Normal cellularity	4	5	6	6	4	5	6	5
(2) Slight hypocellularity	0	0	0	0	0	1	0	1
(1) Moderate hypocellularity	1	0	0	0	1	0	0	0
(0) Severe hypocellularity	1	1	0	0	1	0	0	0
Chondrocyte clustering								
(2) No clusters	2	2	5	5	5	3	3	3
(1) <25% of clusters	4	4	1	1	1	2	3	3
(0) 25–100%of clusters	0	0	0	0	0	1	0	0
4. Freedom from degenerative changes in adjacent cartilage								
(3) Normal cellularity, no clusters, normal staining	0	0	2	5	1	1	4	5
(2) Normal cellularity, mild clusters, moderate staining	1	2	2	1	3	2	1	1
(1) Mild or moderate hypocellularity, slight staining	4	4	2	0	2	2	1	0
(0) Severe hypocellularity, poor or no staining	1	0	0	0	0	1	0	0
5.Subchondral repair bone health								
(3) Normal trabecular bone	1	0	1	1	0	0	0	0
(2) Bone remodel	3	6	1	4	2	3	0	2
(1) Callus	0	0	2	0	3	0	3	2
(0) Fibrous tissue, cyst, detached	2	0	2	1	1	3	3	2
Total score/27 (mean ± 95% C.I.)	9.5 (±4.5)	15.9 (±7.0)#	15.6 (±4.6)§	21.9 (±3.6)*	13.5 (±5.6)	13.7 (±5.1)	16.7 (±3.0)	18.4 (±5.8)
(Min–max)	(3.5–14)	(4–20.5)	(9–19.5)	(17.5–25.5)	(7–18)	(9.5–19)	(13–19.5)	(11–26)

C.I. = Confidence Interval.
* 10K vs distal-hole edge $P = 0.025$.
§ Distal vs proximal-hole edge $P = 0.045$.
# 40K vs proximal-hole edge $P = 0.045$.

The 10K implant elicited bone plate repair and hyaline-like repair in 85% of treated drill holes, but was still in a mid-term repair point after 70 days[27]. The delay in chondrocyte hypertrophy by the 10K implant can be considered a desired effect [Fig. 6], since rapid hypertrophy of cartilage that forms in the subchondral bone area is an impediment to further cartilage repair progression[28]. It has yet to be discovered what factors from the knee microenvironment lead to chondroinduction from remodeling and repairing subchondral bone. Others have shown that soft scaffolds allow a greater degree of chondrogenic differentiation while stiff matrix had an opposite effect, inhibiting chondrogenic differentiation in part due to limited mass transport[29]. Granulation tissue has a soft matrix and some types of granulation tissue may be more conducive to chondroinduction, compared to bone defects that are rapidly filled by a stiff fibrocartilage[14].

Our study had several limitations including the use of 2-hole model[30], with significantly worse proximal hole soft tissue filling and histological scores, but similar bone area fraction % and Col-2-positive % repair compared to distal holes. These effects could potentially be due to local release of pro-inflammatory factors, which inhibit BMSC differentiation to osteoblasts[31–33] and chondrocytes[34]. Catabolic factors could be potentially

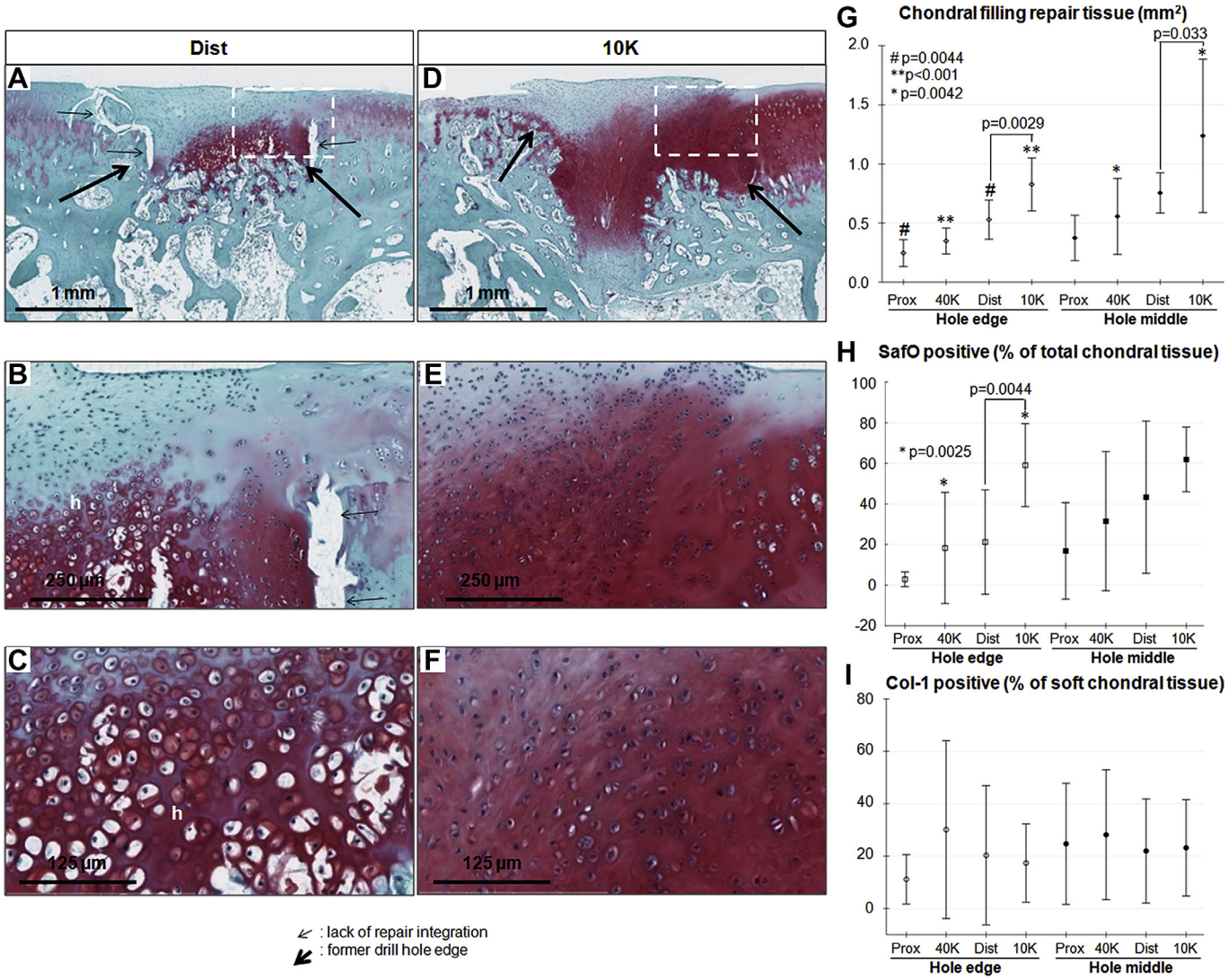

Fig. 6. Effect of implant treatment on soft tissue repair. (A–F) Bilateral distal control and 10K-treated repair tissues from the same animal demonstrating high anabolic response potential through the middle of the hole (SafO/fast green stain), (G) average defect fill, (H) SafO-positive and (I) Col-1-positive soft repair above the osteochondral junction at the hole edge and middle ($N = 6$). Distal control holes showed poor lateral integration and chondrocyte hypertrophy below the osteochondral junction ("h", B–C). 10K implant-treated drill holes had a specifically enhanced lateral integration, delayed chondrocyte hypertrophy (D–F), and anabolic hyaline repair (G–H), with similar levels of collagen type I as drill-only distal holes (I).

released from the supra-patellar synovium and fat pad, or metaphyseal marrow that was found to have an inflammatory reaction specifically below proximal holes at 3 weeks[14]. The transient post-operative knee effusion observed in this study warrants further study in order to fully understand its origins. The delayed effusion may be tied to inflammatory responses to repair soft tissues injured during arthrotomy. Post-surgical drill hole bleeding could also potentially contribute to the observed knee effusion, and the hemostatic properties of chitosan[35,36] could potentially explain the effusion attenuation observed in implant-treated knees. The implant had some practical limitations including a minimal wait-time of 20 min to solidify *ex vivo*; in order to translate this approach to the clinic, we propose that the chitosan-blood mixture should be done while preparing the patient for surgery. Implants can be cut to the required length, and need to be handled in an open petri dish. Our study had low animal numbers ($N = 6$), that were nonetheless sufficient in demonstrating significantly improved repair responses by the 10K implant compared to drill-only. Scaling-up the formulation to large animals and human patients may require different timing of biodegradation *in situ*[15].

Conclusions

Pre-solidified 10K implants are blood clots that contain dispersed ultra-low M_w chitosan microparticles. Press-fitting the 10K implants into aged rabbit knee osteochondral drill holes guides vigorous transient bone-plate resorption and subsequent anabolic WB plate repair with good integration, coupled to hyaline cartilage repair tissue without damaging the adjacent native articular cartilage. In the absence of implant treatment, drill holes repair most frequently with a poorly integrated subchondral bone and a cartilage with low hyaline character.

Author's contributions

Conception and design: CDH, JGM, CHLF. Data acquisition: CDH, JGM, CHLF, GC. JGM and CDH wrote the manuscript. Obtained

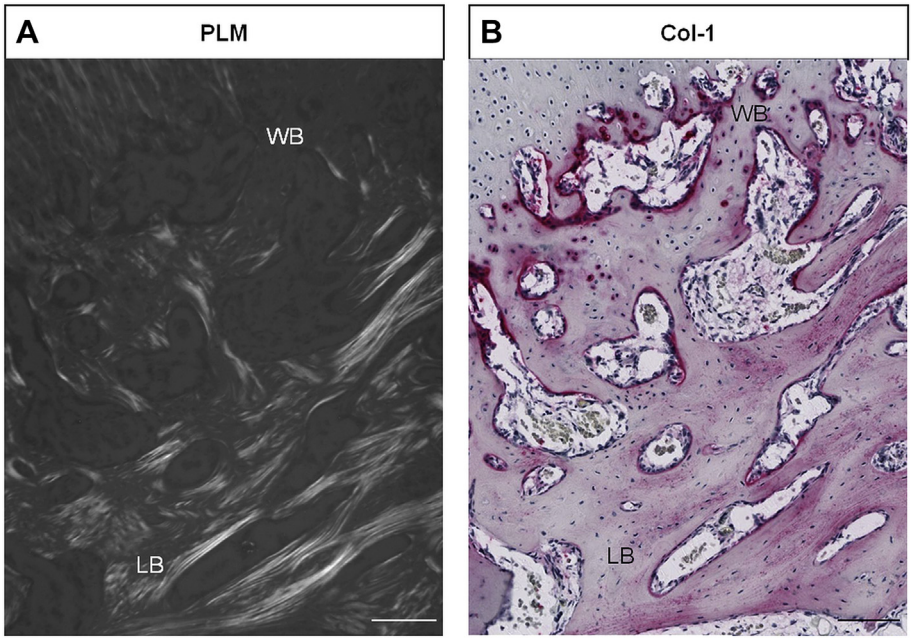

Fig. 7. Example 10K implant-treated drill hole showing area of previous bone plate resorption and repair. (A) PLM and matching Col-1 immunostained section (B, pink) show that repair bone at the top of the hole in contact with the repair cartilage is preceded by vascular invasion, and has WB characteristics, that has matured into birefringent LB deeper in the hole. Scale bar: 100 μm.

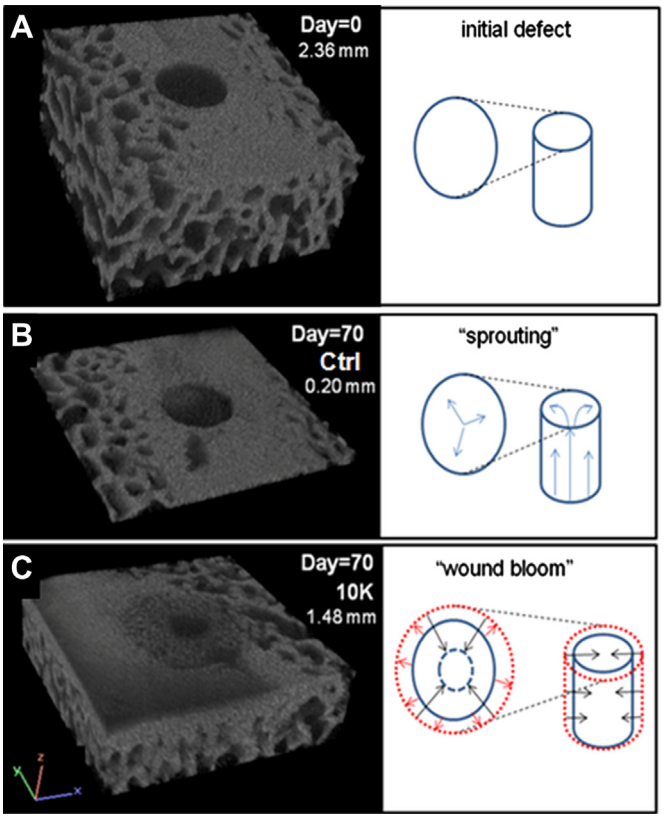

Fig. 8. 3-D micro-CT reconstructions of the initial defect (A), and 70-day mineralized repair in distal control (B) or distal 10K hole (C). The residual drill hole depth (mm) of these example defects is indicated (A–C). Schematics shown on the right illustrate the hole shape and proposed osteochondral repair mechanism. The mechanism in (C) leads to a superior lateral integration of repair bone to native flanking bone plate, and closer proximity of soft repair tissue and native cartilage.

funding for the study: CDH. All authors revised the manuscript critically for important intellectual content, read and approved the manuscript for publication.

Role of the funding source

The funding organizations had no involvement in the study design, in the collection, analysis and interpretation of data, in the writing of the manuscript, or in the decision to submit the manuscript for publication.

Conflict of interest statement

The authors have no competing interests to declare.

Acknowledgments

Funding: Natural Sciences and Engineering Research Council of Canada (NSERC, STPGP 365025), the Canadian Institutes of Health Research (CIHR, 185810-BME), and salary support from the Fonds de Recherche Québec (FRQ-S, National Research Scholar award: CDH), the FQRNT (post-doctoral fellowship, JGM). We thank J Sun, G Picard, and V Darras for valuable technical contributions and J Tremblay for Quality Assurance.

Supplementary data

Supplementary data related to this article can be found at http://dx.doi.org/10.1016/j.joca.2013.12.011.

References

1. Kreuz PC, Erggelet C, Steinwachs MR, Krause SJ, Lahm A, Niemeyer P, *et al.* Is microfracture of chondral defects in the knee associated with different results in patients aged 40 years or younger? Arthroscopy 2006;22:1180–6.
2. Richter W. Mesenchymal stem cells and cartilage in situ regeneration. J Intern Med 2009;266:390–405.

3. Wei X, Messner K. Maturation-dependent durability of spontaneous cartilage repair in rabbit knee joint. J Biomed Mater Res 1999;46:539–48.
4. Chen G, Sun J, Lascau-Coman V, Chevrier A, Marchand C, Hoemann CD. Acute osteoclast activity following subchondral drilling is promoted by chitosan and associated with improved cartilage tissue integration. Cartilage 2011;2:173–85.
5. Meachim G, Emery IH. Quantitative aspects of patello-femoral cartilage fibrillation in Liverpool necropsies. Ann Rheum Dis 1974;33:39–47.
6. Shapiro F, Koide S, Glimcher MJ. Cell origin and differentiation in the repair of full-thickness defects of articular cartilage. J Bone Joint Surg Am 1993;75:532–53.
7. Tran-Khanh N, Chevrier A, Lascau-Coman V, Hoemann CD, Buschmann MD. Young adult chondrocytes proliferate rapidly and produce a cartilaginous tissue at the gel-media interface in agarose cultures. Connect Tissue Res 2010;51:216–23.
8. Hurtig M, Buschmann MD, Fortier LA, Hoemann CD, Hunziker EB, Jurvelin JS, *et al*. Preclinical studies for cartilage repair: recommendations from the International Cartilage Repair Society. Cartilage 2011;2:137–52.
9. Mitchell N, Shepard N. The resurfacing of adult rabbit articular cartilage by multiple perforations through the subchondral bone. J Bone Joint Surg Am 1976;58:230–3.
10. Hoemann CD, Chen G, Marchand C, Tran-Khanh N, Thibault M, Chevrier A, *et al*. Scaffold-guided subchondral bone repair: implication of neutrophils and alternatively activated arginase-1+ macrophages. Am J Sports Med 2010;38:1845–56.
11. Chen H, Chevrier A, Hoemann CD, Sun J, Ouyang W, Buschmann MD. Characterization of subchondral bone repair for marrow-stimulated chondral defects and its relationship to articular cartilage resurfacing. Am J Sports Med 2011;39:1731–40.
12. Miller RE, Grodzinsky AJ, Vanderploeg EJ, Lee C, Ferris DJ, Barrett MF, *et al*. Effect of self-assembling peptide, chondrogenic factors, and bone marrow-derived stromal cells on osteochondral repair. Osteoarthritis Cartilage 2010;18:1608–19.
13. Hoemann CD, Sun J, McKee MD, Chevrier A, Rossomacha E, Rivard GE, *et al*. Chitosan-glycerol phosphate/blood implants elicit hyaline cartilage repair integrated with porous subchondral bone in microdrilled rabbit defects. Osteoarthritis Cartilage 2007;15:78–89.
14. Lafantaisie-Favreau CH, Guzmán-Morales J, Sun J, Chen G, Harris A, Smith TD, *et al*. Subchondral pre-solidified chitosan/blood implants elicit reproducible early osteochondral wound-repair responses including neutrophil and stromal cell chemotaxis, bone resorption and repair, enhanced repair tissue integration and delayed matrix deposition. BMC Musculoeskelet Disord 2013;14.
15. Bell AD, Lascau-Coman V, Sun J, Chen G, Lowerison MW, Hurtig MB, *et al*. Bone-induced chondroinduction in sheep Jamshidi biopsy defects with and without treatment by subchondral chitosan-blood implant: 1-day, 3-week, and 3-month repair. Cartilage 2013;4:131–43.
16. Halim AS, Lim CK. Biomedical-grade chitosan in wound management and its biocompatibility in vitro. In: Elnashar M, Ed. Biopolymers 2010.
17. Oliveira MI, Santos SG, Oliveira MJ, Torres AL, Barbosa MA. Chitosan drives anti-inflammatory macrophage polarisation and pro-inflammatory dendritic cell stimulation. Eur Cell Mater 2012;24:136–53.
18. Simard P, Galarneau H, Marois S, Rusu D, Hoemann CD, Poubelle PE, *et al*. Neutrophils exhibit distinct phenotypes toward chitosans with different degrees of deacetylation: implications for cartilage repair. Arthritis Res Ther 2009;11:R74.
19. Lavertu M, Methot S, Tran-Khanh N, Buschmann MD. High efficiency gene transfer using chitosan/DNA nanoparticles with specific combinations of molecular weight and degree of deacetylation. Biomaterials 2006;27:4815–24.
20. Marchand C, Chen G, Tran-Khanh N, Sun J, Chen H, Buschmann MD, *et al*. Microdrilled cartilage defects treated with thrombin-solidified chitosan/blood implant regenerate a more hyaline, stable, and structurally integrated osteochondral unit compared to drilled controls. Tissue Eng Part A 2012;18:508–19.
21. O'Driscoll SW, Keeley FW, Salter RB. Durability of regenerated articular cartilage produced by free autogenous periosteal grafts in major full-thickness defects in joint surfaces under the influence of continuous passive motion. A follow-up report at one year. J Bone Joint Surg Am 1988;70:595–606.
22. Meretoja VV, Dahlin RL, Wright S, Kasper FK, Mikos AG. The effect of hypoxia on the chondrogenic differentiation of co-cultured articular chondrocytes and mesenchymal stem cells in scaffolds. Biomaterials 2013;34:4266–73.
23. Gan L, Kandel RA. In vitro cartilage tissue formation by co-culture of primary and passaged chondrocytes. Tissue Eng 2007;13:831–42.
24. Seeherman HJ, Li XJ, Bouxsein ML, Wozney JM. rhBMP-2 induces transient bone resorption followed by bone formation in a nonhuman primate core-defect model. J Bone Joint Surg Am 2010;92:411–26.
25. Hadjidakis DJ, Androulakis II. Bone remodeling. Ann N Y Acad Sci 2006;1092:385–96.
26. Re'em T, Witte F, Willbold E, Ruvinov E, Cohen S. Simultaneous regeneration of articular cartilage and subchondral bone induced by spatially presented TGF-beta and BMP-4 in a bilayer affinity binding system. Acta Biomater 2012;8:3283–93.
27. Hoemann CD, Lafantaisie-Favreau CH, Lascau-Coman V, Chen G, Guzmán-Morales J. The cartilage-bone interface. J Knee Surg 2012;25:85–97.
28. Zhang W, Chen J, Zhang S, Ouyang HW. Inhibitory function of parathyroid hormone-related protein on chondrocyte hypertrophy: the implication for articular cartilage repair. Arthritis Res Ther 2012;14:221.
29. Liu SQ, Tian Q, Hedrick JL, Po Hui JH, Ee PLR, Yang YY. Biomimetic hydrogels for chondrogenic differentiation of human mesenchymal stem cells to neocartilage. Biomaterials 2010;31:7298–307.
30. Furukawa T, Eyre DR, Koide S, Glimcher MJ. Biochemical studies on repair cartilage resurfacing experimental defects in the rabbit knee. J Bone Joint Surg Am 1980;62:79–89.
31. Pacifici R. The immune system and bone. Arch Biochem Biophys 2010;503:41–53.
32. Gruber R. Cell biology of osteoimmunology. Wien Med Wochenschr 2010;160:438–45.
33. Gordeladze JO, Reseland JE, Karlsen TA, Jakobsen RB, Engebretsen L, Lyngstadaas SP, *et al*. Bone and cartilage from stem cells: growth optimization and stabilization of cell phenotypes, regenerative medicine and tissue engineering. In: Eberli D, Ed. Cells and Biomaterials. InTech; 2011:588.
34. Heldens GT, Blaney Davidson EN, Vitters EL, Schreurs BW, Piek E, van den Berg WB, *et al*. Catabolic factors and osteoarthritis-conditioned medium inhibit chondrogenesis of human mesenchymal stem cells. Tissue Eng Part A 2012;18:45–54.
35. Millner RW, Lockhart AS, Bird H, Alexiou C. A new hemostatic agent: initial life-saving experience with Celox (chitosan) in cardiothoracic surgery. Ann Thorac Surg 2009;87:e13–4.
36. Whang HS, Kirsch W, Zhu YH, Yang CZ, Hudson SM. Hemostatic agents derived from chitin and chitosan. J Macromol Sci Polymer Rev 2005;C45:309–23.